Journal of Biomolecular NMR, 7 (1996) 121–130
ESCOM

J-Bio NMR 329

Some practical aspects of B_0 gradient pulses

M. Czisch[a], A. Ross[b], C. Cieslar[a] and T.A. Holak[a,*]

[a]*Max-Planck-Institut für Biochemie, D-82152 Martinsried bei München, Germany*
[b]*School of Biochemistry, University of New South Wales, Sydney, New South Wales 2052, Australia*

Received 13 September 1995
Accepted 20 December 1995

Keywords: Gradients; B_0 gradients; Pulsed field gradients

Summary

Pulsed field gradients used together with trim pulses may cause artifacts in NMR spectra that originate from partial refocusing of dephased magnetization. These effects can reduce the efficiency of solvent suppression. The duration of the trim and PFG pulses should be in the range in which refocusing is negligible. Background gradients due to bad shimming also interfere with the B_0 field gradient pulses, producing gradient-recalled echoes that reduce the receiver gain for NMR experiments. The shim settings can be optimized using simple experiments, as described in this paper. Eddy currents that cannot be completely compensated by adjustments of preemphasis induce phase shifts in NMR signals. The decay constants for a given spectrometer setup can easily be measured. If the experiment does not allow for proper compensation delays, the phase of the pulses must be adjusted to compensate for these phase shifts.

Introduction

Pulsed field gradients (PFGs) have been widely used in high-resolution NMR spectroscopy to improve the quality of spectra (Sattler et al., 1995; Stonehouse et al., 1995; for reviews see Hull, 1994; Keeler et al., 1994). However, PFGs can also cause spectral artifacts that originate from their interaction with trim pulses, shim settings, and metallic parts of the spectrometer. In this paper we will discuss the hardware-dependent origins of these artifacts and indicate remedies for their elimination.

Theory

Interference of B_0 gradients and B_1 inhomogeneity

Trim pulses (TPs) and PFGs are frequently combined for removal of unwanted coherences (Bax and Pochapsky, 1992; Keeler et al., 1994). As TPs and PFGs cause dephasing with respect to the two orthogonal axes (e.g. the x- and z-axes, respectively), the resulting defocusing is naively expected to be more efficient; defocusing of the magnetization is no longer restricted to a plane but can cover a globe. We will show that a coherence which is defocused by an inhomogeneous field in one direction, for example TP_x, can be partially refocused by another inhomogeneous magnetic field in an orthogonal direction, for example a B_0 gradient pulse. A necessary requirement for such partial refocusing is that the derivatives of both field inhomogeneities are not orthogonal.

The following coherence transfer is possible for an inhomogeneous trim field pulse $B_x(\vec{r})$, applied for a time t_p (Ernst et al., 1987):

$$I_z \xrightarrow{\beta(\vec{r})I_x} \frac{i}{2} I_+ \sin\beta(\vec{r}) - \frac{i}{2} I_- \sin\beta(\vec{r}) + I_z \cos\beta(\vec{r}) \quad (1)$$

Using the relations

$$\sin\beta(\vec{r}) = \frac{1}{2i}\left(e^{i\beta(\vec{r})} - e^{-i\beta(\vec{r})}\right)$$
$$\beta(\vec{r}) = \omega_p(\vec{r})t_p = -\gamma B_x(\vec{r})t_p \quad (2)$$

where $\omega_p(\vec{r})$ gives the spatial dependent field strength of the rf pulse applied for a time t_p, and neglecting the contribution proportional to I_z, Eq. 1 results in:

*To whom correspondence should be addressed.

$$\frac{1}{4}I_+\left(e^{-i\gamma B_x(\vec{r})t_p} - e^{i\gamma B_x(\vec{r})t_p}\right) \qquad (3)$$
$$-\frac{1}{4}I_-\left(e^{-i\gamma B_x(\vec{r})t_p} - e^{i\gamma B_x(\vec{r})t_p}\right) = \rho_1(\vec{r})$$

If B_x is dependent on z, the resulting coherence has the same spatial dependence as B_x, expressed by the 'phase terms' in Eq. 3. After an inhomogeneous magnetic field with an orthogonal axis of rotation, e.g. a PFG $B_z(\vec{r})$, has been applied for a time t_g, the magnetization $\rho_1(\vec{r})$ evolves according to:

$$\rho_1(\vec{r}) \xrightarrow{B_z(\vec{r})} \frac{1}{4}I_+e^{-i\gamma(B_x(\vec{r})t_p+B_z(\vec{r})t_g)} - \frac{1}{4}I_+e^{i\gamma(B_x(\vec{r})t_p-B_z(\vec{r})t_g)} \qquad (4)$$
$$-\frac{1}{4}I_-e^{-i\gamma(B_x(\vec{r})t_p-B_z(\vec{r})t_g)} + \frac{1}{4}I_-e^{i\gamma(B_x(\vec{r})t_p+B_z(\vec{r})t_g)}$$

Integration over the sample volume gives rise to the observable magnetization, with an amplitude dependent on the duration, strength, and spatial distribution of the B_x and B_z inhomogeneities. As an example, a simple linear model for both inhomogeneous fields of the form

$$B_1(\vec{r}) = (\partial B_x/\partial z)\cdot z = G^{rf}\cdot z$$
$$B_0(\vec{r}) = (\partial B_z/\partial z)\cdot z = G^{PFG}\cdot z \qquad (5)$$

is considered, with G^{PFG} representing the PFG strength (possible imperfections of the homogeneous magnetic field are neglected). After integration along the z-axis of the sample tube (ranging from $-l/2$ to $+l/2$), Eq. 4 results in:

$$-\frac{1}{4}(I^+ + I^-) \quad \text{if} \quad \frac{t_p}{t_g} = \frac{G^{PFG}}{G^{rf}}$$
$$\frac{1}{4}(I^+ - I^-) \quad \text{if} \quad \frac{t_p}{t_g} = -\frac{G^{PFG}}{G^{rf}} \qquad (6)$$

In practice, the inhomogeneities, especially TP, can only be approximated by such a simple model, but since B_1 inhomogeneities are dominated by the transition bands along the z-axes, the model is a good approximation. Nevertheless, refocusing of coherences is imperfect, but the resulting magnetization can be measured easily for a large solvent signal.

Interference of background gradients and B_0 gradients

Partial refocusing of coherences can be accomplished by the interference of the strong defocusing PFGs and weak inhomogeneity of the static external B_0 field (Redfield and Gupta, 1971; Karlicek and Lowe, 1980). This effect is normally minimized by proper setting of the shim parameters. Problems arising from this interference that lead to a reduced suppression factor of unwanted coherences were described previously (Moonen et al., 1992).

In pulse sequences with gradient pulses, distortions in the shapes of FIDs lead to artifacts close to the solvent line. These distortions are usually explained as the interference between the field distribution of the gradient coil and the inhomogeneity of the main field. The static magnetic field in a plane at the coordinate z (with respect to the center of the sample tube) can be written as:

$$B_z(z) = B_0 + \sum_{j=1}^{j_{max}} G_j^{static}\, z^j \qquad (7)$$

Transversal components are neglected for the sake of clarity. G_j^{static} are coefficients of a power series with respect to z. These parameters can be adjusted (normally up to the fourth or fifth order) with shim devices. A perfectly shimmed probe shows only the B_0 component of Eq. 7. A slight missetting of the shim values causes a z-dependent phase shift of the magnetization during delays inserted in the experiment. This line broadening effect is exactly the same as that found during the PFG, but hopefully much weaker. In the experiment consisting of 90° and PFG pulses, directly followed by a detection period, the magnetization (written as a complex vector) at time t (counted from the beginning of the PFG) results from the integral of Eq. 7 over all planes within the sample:

$$\vec{M}(t) = M_0 \int_{-1/2}^{1/2} e^{-i2\pi\gamma B_z(z,t)\,t}\, dz$$
$$= M_0 \int_{-1/2}^{1/2} e^{-i2\pi\gamma\left[B_0 + \sum_{j=1}^{j_{max}}\left(G_j^{static}+G_j^{PFG}(t)\right)\cdot z^j\right]t}\, dz \qquad (8)$$

where $G_j^{PFG}(t)$ represents the coefficients of the power development of the PFG. B_0 is the homogeneous field of the spectrometer. This term gives rise to the precession frequency ω of the signal. The term G_1^{PFG} arises from a linear gradient pulse (Eq. 5) and the term G_1^{static} from background gradients due to imperfect shimming of the z-component (Eq. 7). In practice, refocusing due to higher orders of z is seen in the spectra. After application of a perfectly linear defocusing gradient pulse with strength G_1^{PFG} and duration t_g, and neglecting the static contributions 'under' the gradient, magnetization of the form

$$\vec{M}(t) = M_0 e^{i\omega t}\cdot \int_{-1/2}^{1/2} e^{-i2\pi\gamma\left[\left(G_1^{PFG}\cdot t_g + G_1^{static}t\right)z + \left(\sum_{j=2}^{Jmax} G_j^{static}\cdot z^j\right)t\right]} dz \qquad (9)$$

can be measured. A general analytical solution of Eq. 9 is difficult. However, interference of PFG and linear missetting of the shim can be solved analytically:

$$G_1^{PFG}\cdot t_g = -G_1^{static}\cdot t \qquad (10)$$

A gradient-recalled echo arising from refocusing of the dephased magnetization by the background gradients is refocused after a time period

$$t_{echo} = -G_1^{PFG} t_g / G_1^{static} \quad (11)$$

leading to the distorted shape of the FID. In practice the assumption $G_1^{PFG} \gg G_1^{static}$ holds; therefore the echo of Eq. 11 cannot be detected, as the signal has completely decayed by T_2 relaxation. In a more general form, the different spatial offset z_0 of the PFG coil with respect to the shim coils must be included in Eq. 9. Therefore, the proper form of the integral of Eq. 9 is:

$$\int_{-l/2}^{l/2} e^{-i2\pi\gamma\left[\left(G_1^{PFG} \cdot t_g z + G_1^{static} t(z-z_0)\right) + \left(\sum_{j=2}^{j_{max}} G_j^{static} \cdot (z-z_0)^j\right) t\right]} dz \quad (12)$$

This offset is an important factor, since it determines the location of the gradient-recalled echoes in the frequency domain. Since the integral of Eq. 9 ranges from –l/2 to +l/2, the imaginary part (y-magnetization) will vanish. Fourier transformation of such a FID will result in a doublet, symmetrically located around the central solvent frequency. This condition is no longer fulfilled in Eq. 12, where both magnetization components are time dependent. This precession results in an additional offset of the center of the doublet, as can be seen in Fig. 3. A numerical simulation for a gradient of amplitude G_1^{PFG} and duration t_g and the offset dependence of imperfection of the shim of an arbitrary order is possible by digitizing a tube into N thin planes (compared to the pitch of the dephased magnetization). The signals from all planes can be numerically integrated, resulting in an artificial FID that yields the spectrum after Fourier transformation.

Eddy currents in gradient coils

Eddy currents can be reduced by the use of actively shielded probeheads, proper setting of the preemphasis and shaping of the PFGs (Majors et al., 1990; Keeler et al., 1994). In addition, the induced B_0 shifts can be corrected by applying an appropriate waveform to the shim coils. These can be calculated from a spherical-harmonic expansion of the magnetic fields produced following a gradient pulse (Eccles et al., 1993), or by modulation of the transmitter and receiver reference frequencies (Crozier et al., 1992,1994).

After a PFG, usually a certain delay is incorporated in a pulse sequence before the next rf pulse is applied. This delay (of approximately 100 µs) is necessary because of a delayed ending of the PFG. Even if the PFG is switched off in the pulse program, the current to the gradient coil always persists longer, for several tens of microseconds. This is due to hardware limitations of the amplifiers currently in use (there is also an influence of the gradient coil itself). During this time no rf pulse can be efficiently applied. When the current from the amplifier to the gradient coil has decayed completely, residual eddy currents are still present. The residual eddy currents measured in our actively shielded probehead showed long decay constants compared to the values of a typical compensation delay, which is on the order of hundreds of microseconds. Compared to the PFG itself, the magnetic field caused by eddy currents is small. Experimentally it can be shown that the eddy current field results in a time-dependent phase shift (whereas only minor dephasing related to field inhomogeneity was noticed). To compensate for this effect, the phase of a subsequent rf pulse has to be adjusted. A possible explanation for these effects is a weak gradient field caused by the eddy currents located asymmetrically, with an offset z_0 with respect to the center of the receiver coil (Keeler et al., 1994). If this offset were not present, only minor dephasing of the signals would be seen. This effect can be removed if the gradient unit has a z_0 compensation; otherwise care must be taken in positioning the PFG within a pulse sequence.

The current $I_1(t)$ in the gradient coil induces an eddy current $I_2(t)$ in the metallic parts of the probehead and the magnet. Both currents decay because of the intrinsic resistance R. The transfer from $I_1(t)$ to $I_2(t)$ must be known in order to estimate the distortions. Assuming a single resistance R, the behavior of the system can be described by a single time constant τ_d. The z-dependent field produced by the eddy current immediately after the gradient can be calculated according to:

$$B_{eddy}(0+,z) = k_{eddy}(z) \int_0^{t_g} \frac{\partial I_1(t')}{\partial t'} \cdot e^{-(t'/\tau_d)}\, dt' \quad (13)$$

A simple procedure to measure the constant τ_d is given in the Experimental section. The shape function $k_{eddy}(z)$ cannot be easily measured. The integration of Eq. 13 must be performed over the duration of the gradient pulse (t_g). During a subsequent delay ($I_1 = 0$), the following equation holds:

$$B_{eddy}(t,z) = B_{eddy}(0+,z) \cdot e^{-(t/\tau_d)} \quad (14)$$

If the main effect of the induced field $B_{eddy}(t)$ were dephasing of the signal, the size of a FID excited by a 90° pulse directly after the PFG would be reduced substantially. This is, however, not seen in practice. Nevertheless, the line shape of the Fourier-transformed FID is destroyed completely. The effect can be explained by assuming that the induced gradient causes a time-dependent shift of the offset frequency of the signals.

The on-resonance signal under the time-dependent field $B_{eddy}(t)$ of Eq. 14 can be calculated according to:

$$S(t) \sim \int_{-l/2}^{l/2} e^{-i\gamma_I \int_0^t B_{eddy}(t',z)dt'} dz \qquad (15)$$

The real and imaginary parts of this equation indicate the x- and y-magnetizations, respectively. Using the simple model $k_{eddy}(z) = c*(z-z_0)$, where the zero position of the gradient field with respect to the receiver coil is given by z_0, an analytical solution is possible using Eq. 13:

$$S_x(t) \sim +2 \sin[-A(t)\, l] \cos[A(t) 2\, z_0] / A(t)$$

$$S_y(t) \sim -2 \sin[-A(t)\, l] \sin[A(t) 2\, z_0] / A(t) \qquad (16)$$

$$A(t) = \gamma_I\, c\, B_{eddy}(0+)(1 - e^{-t/\tau_d})\, \tau_d$$

where relaxation effects are neglected. The integration ranges over the detected volume. Equation 16 shows that S_x decays, whereas S_y builds up to a certain value. The measurement of S_y can be used to estimate the decay constant of the eddy current.

The ratio of the two components at time $t \gg \tau_d$ can be calculated from Eq. 16:

$$\phi(t) = \text{arccot}(S_x(t)/S_y(t))$$

$$\phi(t \to \infty) = 2\gamma_I z_0 \tau_d\, c\, B_{eddy}(0+, z=0) \qquad (17)$$
$$= \varepsilon\,(z_0, \text{shape}) \cdot G\,[\text{T/cm}]$$

This shows that the resulting phase shift is linearly dependent on the strength of the PFG since $B_{eddy}(0+, z=0)$ is proportional to this value and also dependent on the PFG shape and on z_0. By measuring ϕ as a function of the PFG strength, the $\varepsilon(z_0, \text{shape})$ can be estimated.

Experimental

All experiments were performed with a triple resonance 5 mm gradient probehead on a Bruker AMX 600 spectrometer, equipped with a BGU II gradient unit.

Interference of B_0 gradients and B_1 inhomogeneity

The pseudo-3D experiment of Fig. 1 was performed to measure the magnetization that was defocused by a trim pulse along the x-axis and refocused by a PFG. Both trim and PFG pulses were incremented. The trim pulse 'p' of variable length t_p (first dimension) was applied on the steady state magnetization I_z, followed by a PFG ('G') with variable duration t_g (second dimension). The gradient was sine shaped (64 points) with a maximal amplitude of 10 G/cm. The data set consisted of 64 t_g increments (maximum t_g 1100 μs) and 70 t_p increments (maximum t_p 3000 μs). The delay Δ was set to 3 ms. A total of 2K data points were acquired. The carrier was set on the strong solvent signal. Four scans without phase cycling were

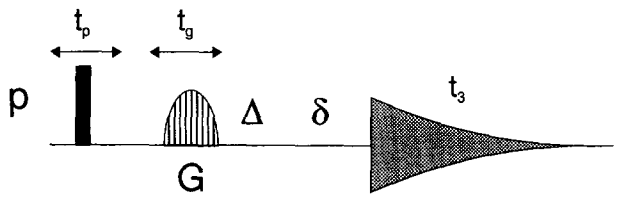

Fig. 1. Pulse sequence for measuring the interferences between the trim pulse (p) and PFG (G) pulses.

summed. The relaxation delay between the scans was chosen to be 1.3 s. The receiver gain was set to 512 units. To ensure a constant duration of the sequence, a delay of $\delta = \delta^0 - t_p - t_g$ (with $\delta^0 = 5$ ms) was employed before opening the receiver. The magnetization was measured during acquisition (third dimension). After Fourier transformation along t_3, the plane of the water signal could be displayed in a 2D plot with axes t_p and t_g. The result is shown in Fig. 2.

Interference of background gradients and B_0 gradients

Figure 3A shows the data set collected with the pulse sequence of Fig. 1, with fixed values for t_p (= 90° pulse) and t_g (1 ms, 10 G/cm, sine shaped). By changing the value of the z^3 shim on the Bruker BSV10 shim unit in 32 equidistant steps, a pseudo-2D spectrum was acquired, collecting 2K data points in a single scan. The receiver gain was set to 4K. The influence of the sign of the PFGs on the gradient-recalled echo in a standard GE-HMQC experiment (Fig. 4C) (Hurd and John, 1991; Davis et al., 1992; Ross et al., 1993) was also determined. An N-type echo was collected with one scan and the strength of the

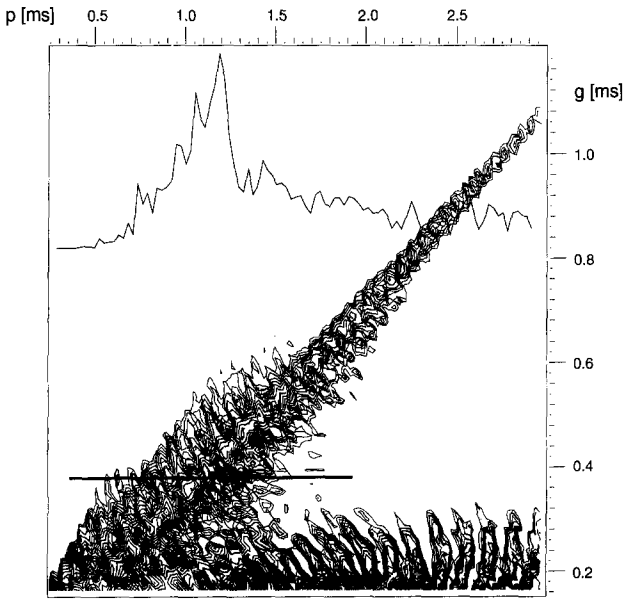

Fig. 2. Plane at the water frequency of the pseudo-3D experiment of Fig. 1, performed on a water sample doped with Cr^{3+}. The contour plot (absolute value) shows partial refocusing of water magnetization. See the text for details. The horizontal bar gives the position of the inserted 1D spectrum.

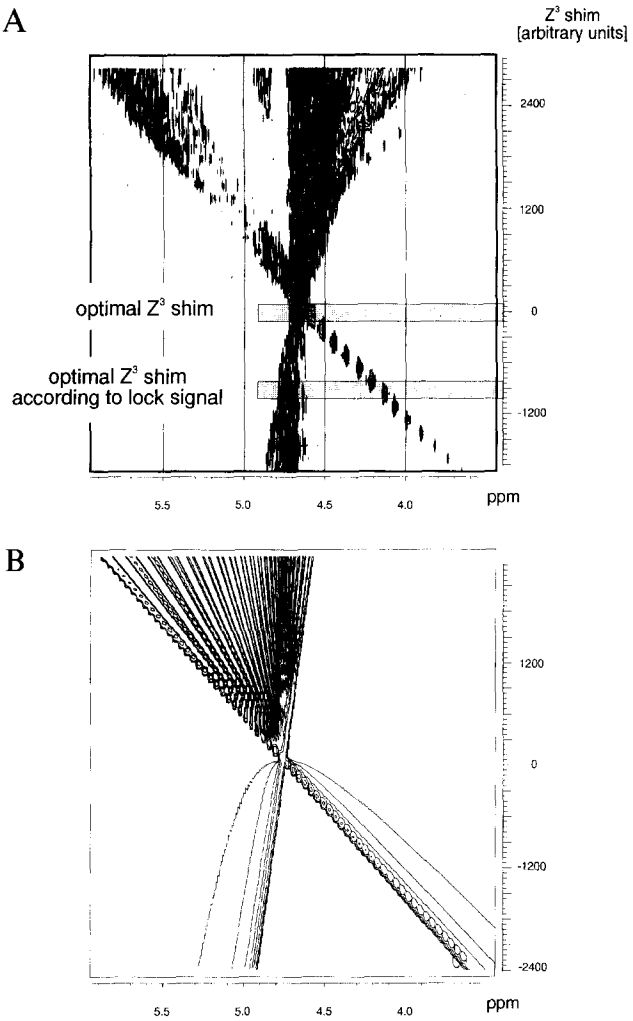

Fig. 3. (A) Data set collected with the pulse sequence of Fig. 1, with fixed values for t_p (90° pulse) and t_g (1 ms, 10 G/cm, sine shaped). By changing the value of the z^3 shim on the Bruker BSV10 shim unit in 32 equidistant steps, a pseudo-2D spectrum was acquired collecting 2K data points in a single scan. Optimized values for the shim setting according to maximum lock signal and our optimization procedure, respectively, are indicated. (B) Numerical simulation of a signal dephased by a gradient linear in z, which was rephased by a z^3 inhomogeneity of the shim. See the text for details.

PFGs G_1:G_2:G_3=+5:+5:+1 and −5:−5:−1, respectively. The distortions introduced by the gradient-recalled echoes can be visualized by inspecting the solvent signal in a 2D HMQC spectrum (Fig. 5).

Eddy currents in gradient coils

The pulse sequence to determine the decay constant of the eddy currents following a rectangular gradient pulse (g, 5 ms, 10 G/cm) is shown in Fig. 6A. The 1° flip angle was chosen to neglect the decay of eddy currents 'under' the rf pulse. t_1 was incremented to monitor the decay of the eddy currents. Parameter Δ_1 was set to 100 μs. A delay of 100 ms ensures that all residual eddy current effects decayed before acquisition. Figure 6B shows the pulse sequence to determine the value given in Eq. 14. Parameter Δ was set to 100 μs. The pulse sequence for demonstrating the effect of the phase shift induced by eddy currents is shown in Fig. 6C. A two-scan reference experiment without the PFGs was performed and phased. The PFGs had a duration of 1 ms each and were sine shaped, with an amplitude of approximately 10 G/cm. The delays were set to 11 ms, including the gradients and compensation. All experiments were performed on a chloroform sample (10% $CHCl_3$, 1% TMS, acetone-d_6).

Results and Discussion

Interference of B_0 gradients and B_1 inhomogeneity

If both the trim and PFG pulses worked in a cooperative manner, only a small signal should be visible in the spectra acquired with the experiment of Fig. 1. This signal is expected to decay rapidly with increasing durations of both pulses. We observed, however, a strong refocused solvent signal (Fig. 2). The presence of the diagonal in Fig. 2 can be explained by the linear model given in Eq. 6, thus reflecting a similar spatial dependence for the two inhomogeneities. It should be noted that the durations of the PFG and trim pulses are within the range often used in NMR experiments. For shorter gradients, the deviation from the diagonal can be explained by imperfect defocusing of the solvent signal. When no PFG is applied, solvent suppression due to the trim pulse alone is weak. The combination of both suppression techniques can lead, however, to even less effective suppression than that due to the PFG alone. Less effective suppression can occur in the case of the heteronuclear experiment that involves the INEPT transfer step with a trim pulse, followed by a zz-filter with the PFG to defocus spins not coupled to the heteronucleus (Bax and Pochapsky, 1992). This is also true for the gradient experiments with an isotropic mixing sequence flanked by trim pulses (Yamazaki et al., 1994).

Interferences between PFGs and the more sophisticated spin-locking sequences such as GARP (Shaka et al., 1985) or MLEV-17 (Bax and Davis, 1985) are minor, since these decoupling sequences are compensated for B_1 inhomogeneities. We carried out an experiment in which a simple trim pulse was replaced by the MLEV-17 sequence (data not shown). Refocusing effects were visible only for gradients shorter than 500 μs and with strengths below 10 G/cm. Longer PFGs lead to perfect removal of residual signals. No 'diagonal' as discussed above was visible. However, for shorter gradients also, nonlinear orders of refocusing appeared. It should also be mentioned that effects described for the B_x and B_z rotations occur for any arbitrary combination of orthogonal rotations having a parallel component of their spatial dependencies. This problem can be reduced by using a three-axis B_0 gradient system or a single magic angle gradient (Bowtell and Peters, 1995), since the interference of the TP with this gradient is expected to be much smaller.

Interference of background gradients and B_0 gradients

Partial refocusing of defocused coherences of the solvent signal by the inhomogeneity of the static magnetic field may cause artifacts in NMR spectra. Since per definition, refocusing of any dephased magnetization can take place in an inhomogeneous B_0 field, this effect can be exploited to further improve the quality of the shim.

Figure 3A shows that the defocused solvent magnetization was partially refocused by the background gradients represented by z^3 shim settings. For perfect defocusing, no residual solvent signal should be visible. However, for each row two signals appeared in Fig. 3A. The shift of the center of the two lines with respect to the frequency of the solvent is proportional to the value of the z^3 shim component. Shape and location are dependent on the setting of all shim parameters and the sign of the PFG. Assuming the presence of an offset between the coils, the qualitative agreement with our numerical simulations can be seen in Fig. 3B. If the relative sign of the PFG and the background gradients (where the latter are set to zero for the optimal shim value) are different, two sharp lines can be detected (Fig. 3B). If the PFG and background gradients have the same sign, the structure of the lines covers a broad frequency range showing reduced intensity (Fig. 3B). We found that a partial refocusing of magnetization was also achieved by any other shim setting that had a z contribution, like for example xz or yz (data not shown). Because of the imperfect orthogonality of the shim coils, a slight influence of x and y would also be possible, but this was not observed in our measurements.

The experiments described above can be used for optimizing the values of some shim currents (e.g. z^4, z^5). The simulation showed that an optimized value is obtained if the location of the echo is 'under' the solvent line (having minimal amplitude), which is also expected from theory. We could not observe any negative (or positive) influence of these settings on the line shapes compared to a non-gradient reference experiment performed on a protein sample. The major advantage of the optimized shim setting lies in the fact that the receiver gain can be optimized, since the maximal signal amplitude is no longer determined by the gradient-recalled echo. The shim values differ from settings found by optimizing the lock signal level (standard shim routine). This is indicated in Fig. 3. Higher orders of the PFG and the shim lead to additional signals and the asymmetric behavior with respect to the

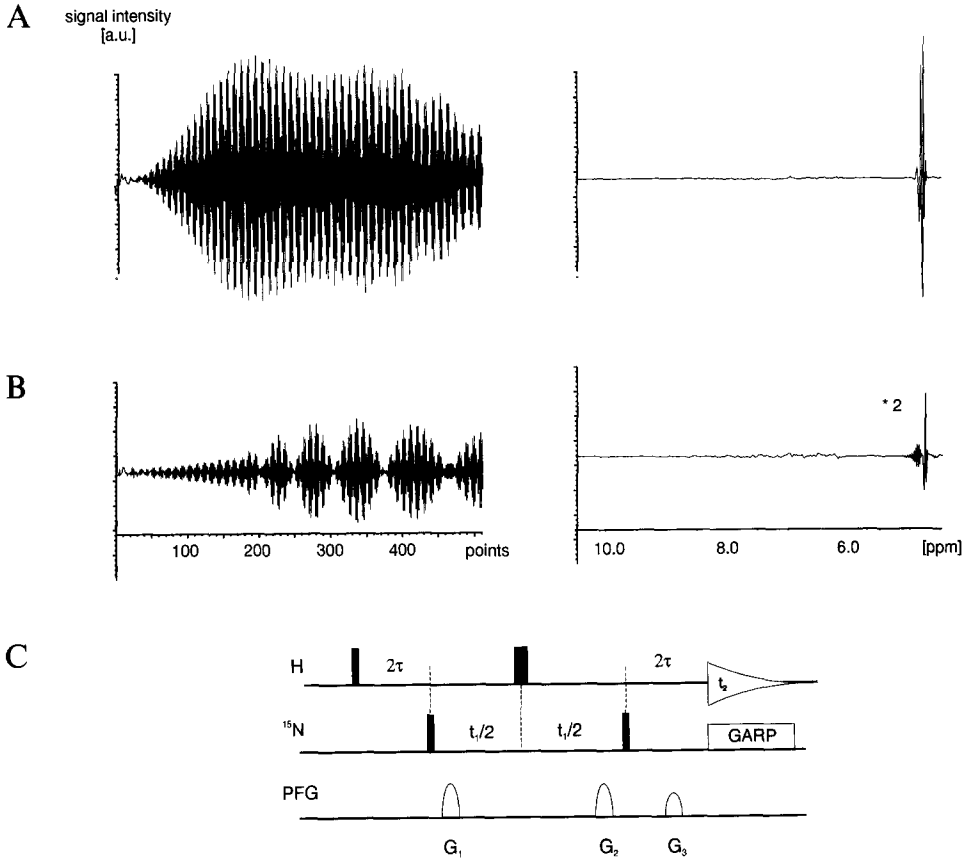

Fig. 4. First t_1 increment of a standard ^{1}H-^{15}N GE-HMQC experiment, showing the FID and the corresponding 1D spectrum. The experiment was performed on a 1 mM 252 amino acid ^{15}N-labeled protein sample dissolved in water at 300 K. An N-type echo was collected in one scan. The setting for the gradients was +5,+5,+1 in (A) and −5,−5,−1 in (B), with all other parameters kept equal. The shim was optimized on the lock level. The gradient-recalled echo is visible in (B). The receiver gain was set to 4K. The spectrum in (B) is scaled by a factor of two compared to that in (A). In (C) the corresponding pulse sequence is given. The delay 2τ was set slightly shorter than $1/2J_{NH}$.

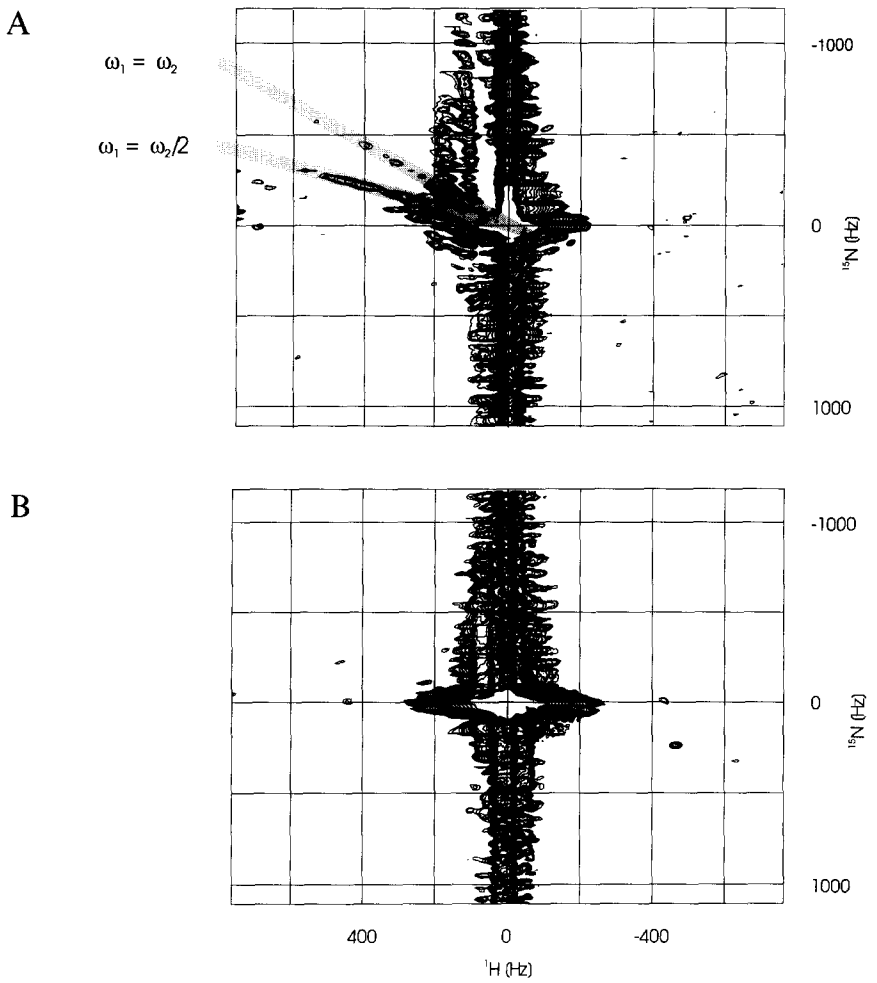

Fig. 5. Residual water resonance extracted from the GE-HMQC spectrum. In (A) two artifacts with 'diagonal behaviour' are visible. The slope is indicated. The artifacts were caused by missetting the z^3 shim value. (B) shows the same spectra with optimized shim values, as described in the text. The distortions shown are clearly above the noise level.

optimized setting visible in Fig. 3. Recently, Van Zijl et al. (1994) introduced a method for optimizing the shim values automatically by mapping the inhomogeneity with imaging methods. These authors also noticed a discrepancy between 'shimming on the lock signal' and an optimized setting of the shim values.

The size of the echo in a pulse sequence that contains rephasing and dephasing PFGs is dependent on the relative setting of the gradient pulses. Figure 4 shows the first t_1 increment of a standard ^{15}N-^{1}H GE-HMQC spectrum (the pulse sequence is given in Fig. 4C) (Hurd and John, 1991; Davis et al., 1992; Ross et al., 1993). In Fig. 4A, the result for the N-type experiment with the gradient setting G_1:G_2:G_3=+5:+5:+1 is shown; in Fig. 4B the setting was G_1:G_2:G_3= −5:−5:−1 for the same N-type selection. In the first case, the shim imperfections lead to partial refocusing of unwanted coherences visible in the sharp, large gradient-recalled echo directly next to the water line, whereas in the experiment depicted in Fig. 4B further defocusing was employed, resulting in a broad echo to the left of the solvent signal. Additional orders of shim inhomogeneities caused a number of gradient-recalled echoes. The location and structure of these echoes were influenced by the setting of all shim parameters.

For pulse sequences with more than one PFG, the interference of any of these pulses with the shim setting must be considered. In the HMQC-type experiment, contributions of the solvent (having their origin in the first 90° pulse) are passed through all PFGs of the sequence and evolve during the t_1 evolution with the offset frequency of the solvent signal from the proton carrier in the F1 dimension. An imperfect 180° pulse in the middle of the sequence creates magnetization influenced by the last two PFGs only. This magnetization experiences only one half of the t_1 evolution, thus showing only half of the frequency of the carrier offset. This behavior is similar to the origin of spectral artifacts as described by Ruiz-Cabello et al. (1992). The position in F2 is given by the positions of the echoes. Both echoes are visible in Fig. 5A, which shows a ^{1}H-^{15}N GE-HMQC spectrum in which only the water line is visible. The echo was caused by purposely missetting the z^3 shim. As shown in Fig. 5B, this distor-

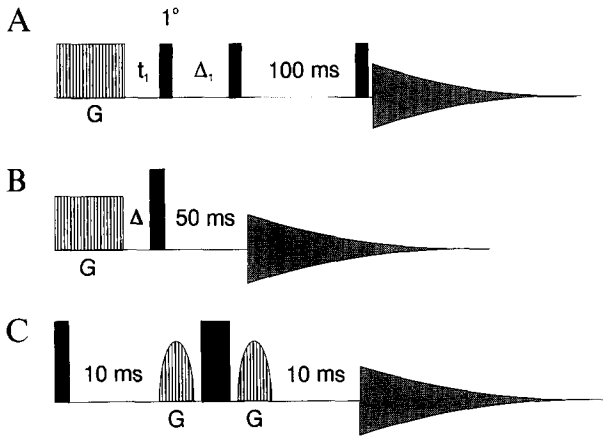

Fig. 6. (A) Pulse sequence to determine the decay constant of the eddy currents following a rectangular gradient pulse (G, 5 ms). The 1° flip angle is chosen to neglect the decay of eddy currents 'under' the rf pulse. (B) Pulse sequence to determine the value given in Eq. 14. Parameter Δ was set to 100 μs. (C) Pulse sequence demonstrating the effect of the phase shift induced by eddy currents.

tion can be reduced by setting the shim according to the method given above. More complex patterns of artifacts are expected for pulse sequences using more PFG pulses or more evolution periods.

It is clear that the artifacts related to refocusing effects can be removed by additional phase cycling of the high-frequency pulses in the pulse sequence. In practice, imperfect setting of shim values is often the limiting factor for increasing the receiver gain in gradient-enhanced experiments. The possible digitization is then determined by the size of the refocused solvent signal. In cases where the shim imperfections cannot be totally removed, it is possible to select the sign of the PFGs such that the solvent signal is further defocused rather than refocused. For the GE-HMQC, this can be achieved if the first and the second PFG are inverted for P- and N-type selection rather than inverting the third pulse (which is responsible for solvent suppression) (Ross et al., 1993). Another possibility is the use of different PFG axes to eliminate gradient-recalled echoes, which was described by Van Zijl et al. (1993) for in vivo HMQC spectroscopy and by Moonen and Van Zijl (1990) for improved water suppression in proton in vivo spectroscopy.

Eddy currents in gradient coils

Eddy currents in PFG experiments cause mainly time-dependent phase shifts of signals. The PFGs must be placed in the pulse sequence at places where this phase shift does not produce line distortion or reduction of amplitude in the spectra. Three experiments were performed to determine τ_d and the dependence of phase errors on the PFG strength.

The first experiment was used to determine the decay constant τ_d of the eddy currents in a probehead (Fig. 6A). The magnetization developed according to Eq. 16. As the carrier was positioned on-resonance at the frequency of

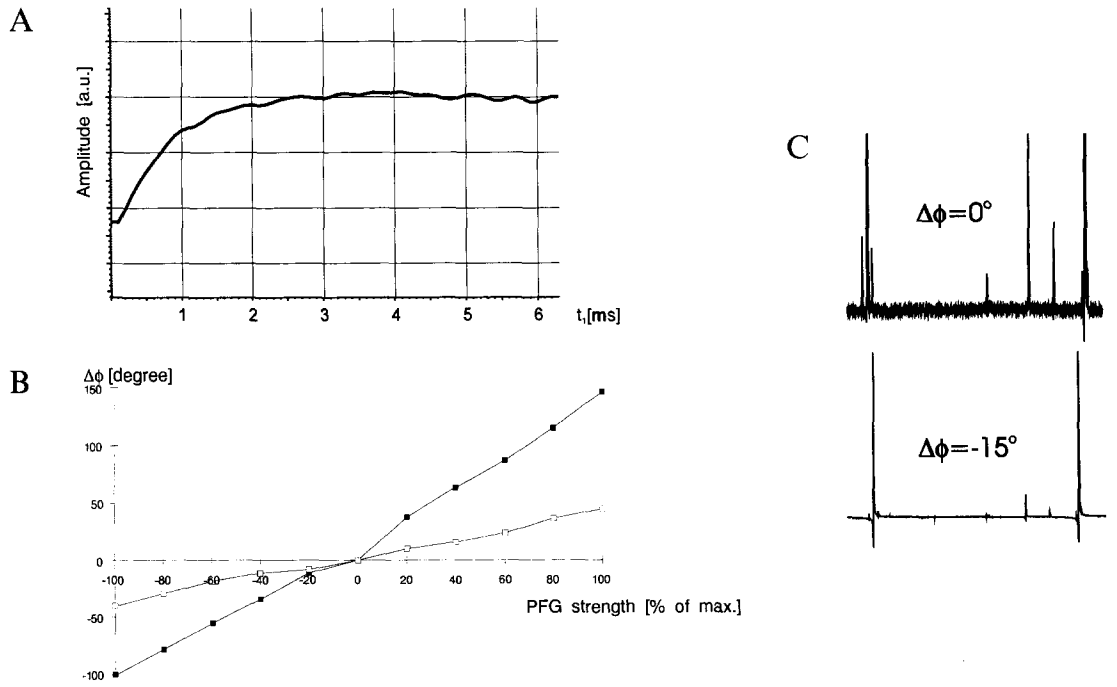

Fig. 7. (A) Intensity of the water resonance as a function of the compensation delay t_1 of the sequence described in Fig. 6A (see the text for details). Note that excitation directly after the gradient pulse is not possible. The decay constant could be extracted from the envelope of the signal. (B) Phase shift induced in the spectrum due to eddy currents measured with the pulse sequence of Fig. 6B. The phase shift relative to a non-gradient reference experiment is given for several PFG strengths. Filled squares represent a 5 ms PFG and open squares a 1 ms PFG. The phase shift in the spectrum was acquired using the pulse sequence of Fig. 6C. The upper entry gives a reference spectrum without gradients, recorded with a two-step phase cycling. The zero order phase shift in the lower spectrum is −15°.

chloroform, no signal should be observed, provided that the second pulse is in quadrature to the first one. The result of the experiment can be seen in Fig. 7A, where the amplitude of the y-magnetization after the delay Δ_1 as a function of t_1 is shown. From the curve in Fig. 7A, the decay constant was estimated to be 600–800 μs. The compensation delay applied after the PFG is frequently determined by inspection of the shapes of FIDs. Typical compensation delays of 100–200 μs are obtained by this method. Our experiment gave much longer times.

Figure 6B shows the second pulse sequence, used to demonstrate the effect of eddy currents on the phase of the signal. A rectangular PFG was followed by a compensation delay of 100 μs and an excitation pulse. The phase shift was allowed to develop during a delay of 50 ms. The phase error $\phi(t\rightarrow\infty)$, which is acquired by the signal due to the z_0 offset, is shown for several PFG strengths in Fig. 7B. The lengths of the rectangular PFGs were 5 and 1 ms. The phase shift of the latter is smaller due to partial self-compensation of the eddy currents, induced by the rising and decreasing flanks of the PFG (an effect that is also exploited by the so-called 'sandwich pulses' (Dötsch et al., 1994; Wider et al., 1994)). At 5 ms the eddy currents on the rising flank had decayed, therefore only the eddy currents of the decay needed to be considered. The result is in agreement with Eq. 16 with $\tau_d = 600$ μs. $\varepsilon(z_0$, 'rectangle') could be estimated to be 15° cm/G.

Finally, the third experiment was performed to show the phase shift in a spin-echo scheme (Fig. 6C). After excitation, a spin-echo sequence was performed before acquisition. The central 180° pulse is flanked by two sine-shaped PFGs, which compensate each other. The phase shift induced to the spin system by the first eddy current is not compensated by the phase shift of the second eddy current. This is because the current had not sufficiently decayed when the 180° pulse was applied, and was added to the second eddy current. A reference experiment without PFGs was also performed (Fig. 7C).

If the gradient is followed by the rf pulse or by acquisition of the signal, the eddy currents should be allowed to decay during a delay of at least 1–2 ms. This is not always possible, e.g. when a PFG is located in an evolution period that should be kept as short as possible for the first increment. In this case it must be ensured that the phase shift of the gradient is the same for all subsequent evolution increments (Tyburn et al., 1992). The gradient should then be located at the end of the evolution period, close to the subsequent rf pulse. This positioning, however, might introduce a signal decay during the evolution period due to diffusion effects (Ruiz-Cabello et al., 1992) if another PFG were used at the beginning of the evolution period.

When the PFG gradient is applied within a constant delay, an additional constant phase shift results. This may cause loss of intensity when 'reading' refocused magnetization with a subsequent pulse. This situation arises in the INEPT transfer steps, where the two 90° pulses applied on the I spin must be orthogonal to allow maximal transfer to the S spin. PFGs can be incorporated to remove imperfection of the 180° pulse, as described by Bax and Pochapsky (1992). Phase shifts can be compensated by locating PFGs directly after the first 90° pulse and the 180° pulse, respectively ($90_I - G - \Delta - 180_{I,S} - G - \Delta - 90_{I,S}$). If the available delay Δ were to become too short for a proper eddy current decay (e.g. in a ^1H-^{13}C INEPT transfer, where the total time $(G - \Delta)$ is set to ~1.9 ms), eddy currents would have to be minimized by shortening or shaping the PFG and/or applying it at a low power. If the strength of the gradient were critical for dephasing at this location, the phase of the reading pulse could be adjusted to compensate for the phase shift of the resonances. Since the described phase shift depends on the gyromagnetic ratio of the nucleus, it will cause problems mainly if proton magnetization is subjected to the gradient dephasing.

Conclusions

The effects discussed in this paper are dependent on individual probeheads and gradient devices. We have shown a number of simple experiments for determining the relevant parameters that allow detection of these effects. We have also shown that PFGs can interfere with trim pulses, thus partly refocusing the dephased magnetization. This effect can decrease the quality of solvent suppression when sequences with additional trim pulses are used. In such cases, one has to ensure that the durations of the trim pulse and the PFG are in the range in which negligible refocusing takes place. Otherwise, removal of one of the pulse components is recommended.

The frequently used shim routine of optimizing the lock signal level does not necessarily lead to optimized performance for gradient experiments. Refocused gradient echoes during acquisition due to missetting will lead to a decrease in the receiver gain. In experiments without additional phase cycling, distortions will be visible around the solvent line. Since the refocusing of the solvent signal depends strongly on the sign of the PFG, one should take care that no gradient-recalled echoes are recorded. We present a method to improve the shim values based on the location of these echoes; using this procedure, an optimized receiver gain can be used. No negative effect was visible on the line shapes in our experiments.

The decay constant of eddy currents induced by PFG was measured for our gradient setup. These are on the order of several hundred microseconds and cannot be totally compensated by the preemphasis adjustment. Since the typical compensation delay after a PFG often must be as short as possible, the PFG should be located in pulse sequences in such a place that the resulting phase shifts

would not influence the experiment. Another possibility would be the adjustment of the phases of rf pulses to compensate these phase shifts as, for example, in INEPT transfer steps.

Acknowledgements

We thank Tim Mather for stimulating discussions. This work was supported by the Deutsche Forschungsgemeinschaft (Project B11, Sonderforschungsbereich 266 of the Technical University of Munich).

References

Bax, A. and Davis, D.G. (1985) *J. Magn. Reson.*, **65**, 355–360.

Bax, A. and Pochapsky, S.S. (1992) *J. Magn. Reson.*, **99**, 638–643.

Bowtell, R. and Peters, A. (1995) *J. Magn. Reson. Ser. A*, **115**, 55–59.

Crozier, S., Eccles, C.D., Beckey, F.A., Field, J. and Doddrell, D.M. (1992) *J. Magn. Reson.*, **97**, 661–665.

Crozier, S., Beckey, F.A., Eccles, C.D., Field, J. and Doddrell, D.M. (1994) *J. Magn. Reson. Ser. B*, **103**, 115–119.

Davis, A.L., Keeler, J., Laue, E.D. and Moskau, D. (1992) *J. Magn. Reson.*, **98**, 207–216.

Dötsch, V., Wider, G. and Wüthrich, K. (1994) *J. Magn. Reson. Ser. A*, **109**, 263–264.

Eccles, C.D., Crozier, S., Westphal, M. and Doddrell, D.M. (1993) *J. Magn. Reson. Ser. A*, **103**, 135–141.

Ernst, R.R., Bodenhausen, G. and Wokaun, A. (1987) *Principles of Nuclear Magnetic Resonance in One and Two Dimensions*, Oxford University Press, Oxford, U.K.

Hull, W.E. (1994) In *Two-dimensional NMR Spectroscopy* (Eds., Croasmun, W.R. and Carlson, R.M.K.), VCH, New York, NY, pp. 186–193.

Hurd, R.E. and John, B.K. (1991) *J. Magn. Reson.*, **91**, 648–653.

Karlicek Jr., R.F. and Lowe, I.J. (1980) *J. Magn. Reson.*, **37**, 75–91.

Keeler, J., Clowes, R.T., Davis, A.L. and Laue, E.D. (1994) *Methods Enzymol.*, **239**, 145–206.

Majors, P.D., Blackley, J.L., Altobelli, S.A., Caprihan, A. and Fukushima, E. (1990) *J. Magn. Reson.*, **87**, 548–553.

Moonen, C.T.W. and Van Zijl, P.C.M. (1990) *J. Magn. Reson.*, **88**, 28–41.

Moonen, C.T.W., Sobering, G., Van Zijl, P.C.M., Gillen, J., von Kienlin, M. and Bizzi, A. (1992) *J. Magn. Reson.*, **98**, 556–575.

Redfield, A.G. and Gupta, R.K. (1971) *Adv. Magn. Reson.*, **5**, 81–113.

Ross, A., Czisch, M., Cieslar, C. and Holak, T.A. (1993) *J. Biomol. NMR*, **3**, 215–224.

Ruiz-Cabello, J., Vuister, G.W., Moonen, C.T.W., Van Gelderen, P., Cohen, J.S. and Van Zijl, P.C.M. (1992) *J. Magn. Reson.*, **100**, 282–302.

Sattler, M., Schwendinger, M.G., Schleucher, J. and Griesinger, C. (1995) *J. Biomol. NMR*, **6**, 11–22.

Shaka, A.J., Barker, P.B. and Freeman, R. (1985) *J. Magn. Reson.*, **64**, 547–552.

Stonehouse, J., Clowes, R.T., Shaw, G.L., Keeler, J. and Laue, E.D. (1995) *J. Biomol. NMR*, **5**, 226–232.

Tyburn, J.-M., Brereton, I.M. and Doddrell, D.M. (1992) *J. Magn. Reson.*, **97**, 305–312.

Van Zijl, P.C.M., Chesnick, A.S., DesPres, D., Moonen, C.T.W., Ruiz-Cabello, J. and Van Gelderen, P. (1993) *Magn. Reson. Med.*, **30**, 544–551.

Van Zijl, P.C.M., Sukumar, S., O'Neil Johnson, M., Webb, P. and Hurd, R.E. (1994) *J. Magn. Reson. Ser. A*, **111**, 203–207.

Wider, G., Dötsch, V. and Wüthrich, K. (1994) *J. Magn. Reson. Ser. A*, **108**, 255–258.

Yamazaki, T., Lee, W., Arrowsmith, C.H., Muhandiram, D.R. and Kay, L.E. (1994) *J. Am. Chem. Soc.*, **116**, 11655–11666.